point that he offered to Hilbert a reconciliation (*22*):

There has been a certain resentment between us, the cause of which I do not want analyze any further. I have fought against the feeling of bitterness associated with it, and with complete success. I again think of you with undiminished kindness and I ask you to attempt the same with me. It is objectively a pity if two guys that have somewhat liberated themselves from this shabby world are not giving pleasure to each other.

In the printed version of his paper, Hilbert added a reference to Einstein's conclusive paper and a concession of the latter's priority: "The differential equations of gravitation that result are, as it seems to me, in agreement with the magnificent theory of general relativity established by Einstein in his later papers" [(*3*), p. 404]. If Hilbert had only altered the dateline to read "submitted on 20 November 1915, revised on [any date after 2 December 1915, the date of publication of Einstein's conclusive paper]," no later priority question could have arisen.

REFERENCES AND NOTES

1. The conclusive paper is A. Einstein, *Sitzungsber. Preuss. Akad. Wiss.* **1915**, 844 (1915).
2. For a historical review, based on joint work with M. Janssen, J. Norton, and J. Stachel, see J. Renn and T. Sauer, *Phys. Bl.* **52**, 865 (1996).
3. The conclusive paper is D. Hilbert, *Nach. Ges. Wiss. Goettingen* **1916**, 395 (1916).
4. For historical reviews, see (*23*); M. J. Mehra, *Einstein, Hilbert, and the Theory of Gravitation* (Reidel, Dordrecht, Netherlands, 1974); and J. Earman and C. Glymour, *Arch. Hist. Exact. Sci.* **19**, 291 (1978).
5. A. Fölsing, *Albert Einstein: A Biography* (Viking, New York, 1997). pp. 375–376. The translation has been slightly modified.
6. Hilbert used the trace of the Ricci tensor (*3*), whereas Einstein used the trace of the matter tensor (see Eq. 1); but these two forms are essentially equivalent.
7. See, for example, A. Pais, *"Subtle is the Lord. . .": The Science and the Life of Albert Einstein* (Oxford Univ. Press, New York, 1982), pp. 257–261.
8. A. Einstein, *Sitzungsber. Preuss. Akad. Wiss.* **1915**, 799 (1915).
9. Staats- und Universitätsbibliothek Göttingen (Handschriftenabteilung), Cod. Ms. D. Hilbert 634.
10. Hilbert republished his paper (*3*) with extensive changes in *Math. Ann.* **92**, 1 (1924).
11. Einstein's paper (*1*) is cited on p. 395 of (*3*), as noted by Guth (*23*).
12. Pages 3 and 4 of the proofs (*9*); translation of this and the following quotations is by the authors.
13. Page 7 of the proofs (*9*).
14. D. Hilbert, letter to F. Klein, 7 March 1918, in *Der Briefwechsel David Hilbert—Felix Klein (1886–1918)*, G. Frei, Ed. (Vandenhoeck and Ruprecht, Göttingen, 1985), p. 129.
15. D. Hilbert, *Nach. Ges. Wiss. Goettingen* **53**, 61 (1917).
16. For a discussion of Hilbert's revised definition of causality and its implications for the Cauchy problem in general relativity, see J. Stachel, in *Studies in the History of General Relativity (Einstein Studies Vol. 3)*, J. Eisenstaedt and A. J. Kox, Eds. (Birkhäuser, Boston, 1992), p. 407.
17. Hilbert denotes the Ricci tensor by $K_{\mu\nu}$ and its trace by K. He does not note the negative value of the determinant of the metric tensor g until later (*10*).
18. D. Hilbert, letter to A. Einstein, 14 November 1915, Einstein Archives Call No. 13-052. We understand that this and the letters referred to in the following will be published in the forthcoming volume 8 of the *Collected Papers of Albert Einstein.*
19. A. Einstein, letter to D. Hilbert, 15 November 1915, Einstein Archives Call No. 13-089.
20. _____, letter to D. Hilbert, 18 November 1915, Einstein Archives Call No. 13-091.
21. _____, *K. Pr. Akad. Wiss. Sitz.* **1915**, 778 (1915).
22. _____, letter to D. Hilbert, 20 December 1915, Einstein Archives Call No. 13-093.
23. E. Guth, in *Relativity*, M. Carmeli *et al.*, Eds. (Plenum, New York, 1970), p. 161.

24. The authors wish to thank G. Castagnetti for his cooperation in the archival work, especially in the dating of the central documents. They also thank P. Damerow, M. Janssen, U. Majer, D. Rowe, and T. Sauer for helpful discussions. We also thank Z. Rosenkranz and the Einstein Archives, The Hebrew University of Jerusalem, Israel, for permission to quote from Einstein's letters, and the Staats- und Universitätsbibliothek Göttingen (*Handschriftenabteilung*) for the kind permission to reproduce Fig. 1.

7 August 1997; accepted 12 October 1997

Warming Early Mars with Carbon Dioxide Clouds That Scatter Infrared Radiation

François Forget and Raymond T. Pierrehumbert

Geomorphic evidence that Mars was warm enough to support flowing water about 3.8 billion years ago presents a continuing enigma that cannot be explained by conventional greenhouse warming mechanisms. Model calculations show that the surface of early Mars could have been warmed through a scattering variant of the greenhouse effect, resulting from the ability of the carbon dioxide ice clouds to reflect the outgoing thermal radiation back to the surface. This process could also explain how Earth avoided an early irreversible glaciation and could extend the size of the habitable zone on extrasolar planets around stars.

It is most likely that the martian atmosphere 3.8 billion years ago was composed primarily of CO_2, with a surface pressure ranging from a few hundred to several thousand millibars, and some H_2O (*1*). At that time, the solar luminosity was about 25% lower than it is at present. Under such conditions, calculations performed with a one-dimensional (1D) climate model by Kasting (*2*) showed that the atmospheric CO_2 should condense in the atmosphere for surface pressures larger than a few tens of millibars. Kasting found that the condensation of CO_2 decreases the atmospheric temperature lapse rate and reduces the magnitude of the greenhouse effect, making it impossible to warm the surface of Mars enough to allow the presence of fluid water together with a CO_2-H_2O gaseous atmosphere. Several alternative mechanisms such as geothermal heating (*3*), an early more massive sun (*4*), or the greenhouse effect of methane (*5*) and ammonia (*6*) have been considered but none has provided a likely solution to the early Mars climate enigma (*5*).

Another consequence of the condensation of CO_2 is the formation of CO_2 ice clouds. Because they are perfect scatterers at solar radiation wavelengths, the CO_2 ice particles should raise the planetary albedo. In the thermal infrared (IR), CO_2 ice is at least 500 times more transparent than water ice, except near 15 μm where the ν_2 absorption band is located and above 90 μm where two broad lattice vibration bands were measured (*7*). Thus, CO_2 ice clouds should not be able to contribute to an absorption-emission greenhouse effect as cirrus clouds on Earth do. On this basis, Kasting (*2*) estimated that CO_2 ice clouds should cool the planet through reflection of sunlight uncompensated by IR trapping.

We have studied the IR properties of the CO_2 ice clouds using a two-stream, hemispheric mean, source function code that allows for multiple scattering, absorption, and emission by atmospheric particles (*8*). The CO_2 ice particle single-scattering properties were obtained from the refractive index measured by Hansen (*7*), using Mie theory with a modified gamma size distribution of effective variance 0.1 (*9*). As expected by Kasting, a cloud composed of CO_2 ice particles smaller than a few micrometers should be almost transparent in the IR, except near 15 μm. However, larger particles can be expected in CO_2 ice clouds. Crystal size is determined by the time required for crystal growth versus the time it takes for the particles to fall out of a supersaturated layer (sedimentation). On Earth, despite the fact that the growth of water ice particles is limited by the diffusion of water vapor through air, particles 80 μm or larger are often observed in cirrus ice clouds, and the observed radiative properties of Earth's cirrus clouds can be fit by assuming equiv-

F. Forget, Laboratoire de Météorologie Dynamique du CNRS, Université Pierre et Marie Curie, Boite Postale 99, 4 place Jussieu, 75252 Paris Cedex 05, France. E-mail: forget@lmd.jussieu.fr
R. T. Pierrehumbert, Department of Geophysical Sciences, University of Chicago, Chicago, IL, USA.

alent spheres with a radius of 16 μm (*10*) with optical depth up to 30. On early Mars, because it is the primary atmospheric constituent that is condensing, the CO_2 cloud particles should grow faster for a comparable sedimentation rate (*11*). Although not much is known about the exact microphysical processes involved, particle radii from 10 to about 100 μm can be expected (*12*). Such particles can more readily scatter the IR radiation (Fig. 1). A cloud composed of such particles would be able to scatter the IR radiation back to the ground and thus contribute to surface warming. IR scattering by clouds or aerosols is not important on Earth, but its warming effect has been considered for other planets (*13*). It has been studied as a means of accounting for the observed IR spectrum of Mars (*14*), Venus (*15*), and even Titan (*16*). In particular, CO_2 ice clouds that scatter IR radiation are thought to have an impact on the radiative budget of the polar regions of Mars at the present time (*17*).

We included the effect of the CO_2 ice clouds in the 1D radiative-convective model designed for early Mars by Kasting (*2*). In the IR wavelength, this model is based on a traditional radiative transfer band model. To account for scattering by CO_2 ice clouds, we used the multiple scattering code and assumed that the effect of a given cloud could be mimicked in the band model by a single-layer cloud with the same transmissivity, reflectivity, and emissivity (*18*). At solar wavelengths, we used a δ-Eddington code to compute multiple scattering by the CO_2 ice particles consistently with Rayleigh scattering by the CO_2 gas molecules, and the system was integrated to radiative-convective equilibrium with the use of a straightforward time-stepping method (*19*). Overall, this climate model gives results similar to the model of Kasting (*2*) when the cloud optical depth is set to zero. When a cloud composed of particles with radii larger than 6 to 8 μm is included, the model predicts a warming of the troposphere and the surface (Figs. 2 and 3). Such a warming may seem surprising because one would expect the IR scattering–induced warming to be balanced by a strong cooling due to scattering of sunlight. In fact, the two effects are not compensating. At solar radiation wavelengths, the importance of the clouds is limited by the fact that the planetary albedo without clouds is already quite high because of Rayleigh scattering in the clear atmosphere (the Rayleigh scattering coefficient for CO_2 is 2.5 times that for air on Earth), whereas in the IR the CO_2 clouds tend to block the outgoing thermal radiation at wavelengths where it would otherwise freely escape. For instance, the planetary albedo (A) of Mars with a 2-bar cloud-free CO_2 atmosphere would be $A_{clear} = 0.38$. The cloud of Fig. 1 increases the planetary albedo to $A_{cloudy} = 0.65$, reducing the absorbed solar energy by about 40% while trapping more than 60% of the outgoing thermal radiation (Fig. 3B). The cloud reduces the outgoing thermal radiation by reflecting the IR flux from below on the one hand, and by absorbing it and reemitting at a lower temperature on the other hand. This last effect corresponds to the "conventional" cloud greenhouse effect that is observed for terrestrial clouds. However, because the cloud can only emit where the atmosphere is opaque, the absorption-emission radiative forcing of CO_2 clouds is almost negligible (Fig. 3B), except for a few watts per square meter in the 15-μm band wings. Consequently, the cloud-induced warming does not depend on the cloud temperature. Thus, it is almost insensitive to the cloud altitude, except when the cloud is artificially put near the surface. In the lower troposphere, the vertical heat transport due to convection and turbulence is larger than the radiative heat flux, and the model predicts a reduced cloud-induced warming. In reality, however, CO_2 clouds should be higher, at the level where condensation temperatures are reached (Fig. 2).

If the early martian atmosphere was in contact with water on the surface, the atmosphere probably contained enough water to increase the IR opacity of the atmosphere (*20*). Assuming a fully saturated troposphere, the greenhouse effect is strongly increased, especially for high surface temperatures (Fig. 2 and Fig. 3A). Water clouds, or possibly CO_2-H_2O clathrate hydrate clouds, probably formed below and within the CO_2 ice cloud layer. With CO_2 ice clouds above, their impact on the planetary albedo was probably small. However, they may have contributed to the greenhouse effect by their IR absorption. Calcu-

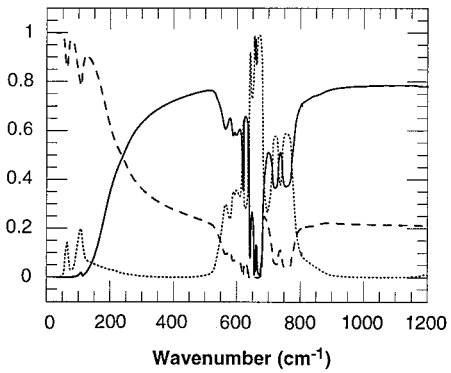

Fig. 1. The reflectivity α (solid curve), transmissivity β (dashed curve), and emissivity ε (dotted curve) of a pure CO_2 ice cloud ($r = 10$ μm) of $\tau = 10$, corresponding to a mass of CO_2 ice about 100 g m^{-2}. Except in the far IR where the cloud particles are too small to scatter the radiation, and near the 15-μm CO_2 absorption band, the main effect of the cloud is a reflection of the IR radiation.

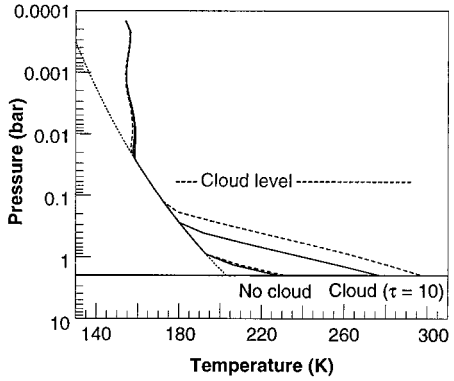

Fig. 2. Calculated mean temperature profiles for a 2-bar CO_2 atmosphere, assuming a 25% reduced solar luminosity corresponding to the early Mars conditions. The effect of the cloud from Fig. 1 ($\tau = 10$, $r = 10$ μm) is shown in the cases of a wet (fully saturated troposphere; dashed curves) and a dry (solid curves) atmosphere. The dotted curve shows the CO_2 condensation temperature profile.

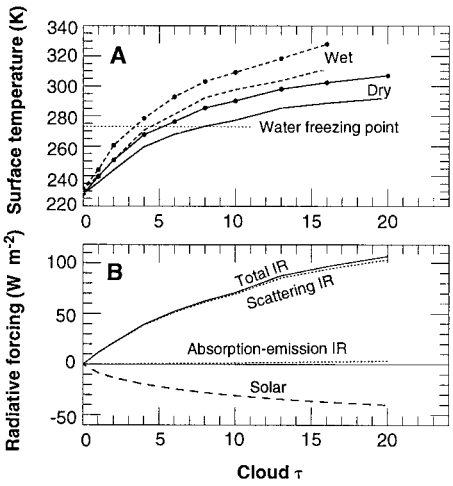

Fig. 3. (**A**) Calculated surface temperature as a function of the cloud τ for $r = 50$ μm (curves with dots) and $r = 10$ μm (curves without dots) in the cases of a wet (dashed curves) or dry (solid curves) 2-bar CO_2 atmosphere on Mars. A 25% reduced luminosity is assumed. (**B**) The corresponding cloud radiative forcings with $r = 10$ μm. The surface warming results from the excess of radiative forcing in the IR as compared with the negative solar forcing. The radiative forcings were defined as $\Delta F_{Sol} = S(A_{clear} - A_{cloudy})$ and $\Delta F_{IR} = F_{clear} - F_{cloudy}$, with S the mean incoming solar flux and F the outgoing thermal fluxes computed in the clear-sky and cloudy-atmosphere cases. The scattering component of ΔF_{IR} was computed assuming that it was proportional to $\alpha I_{subcloud}$ at every wavelength, with $I_{subcloud}$ the upward radiance from the subcloud atmosphere. Similarly, the absorption-emission component was assumed to be proportional to $\varepsilon[I_{subcloud} - B(T_{cloud})]$, with $B(T_{cloud})$ the Planck function at the cloud temperature.

lations performed with water ice particles mixed with the CO_2 ice particles in the modeled cloud reveal a possible warming due to an increase of the absorption-emission cloud radiative forcing, uncompensated by the decrease of the IR scattering forcing (*21*).

Overall, even in the absence of other greenhouse gases except CO_2 and H_2O, the magnitude of the total greenhouse effect of the early Mars atmosphere should have been relatively strong, depending on the assumed humidity, CO_2 and H_2O cloud properties, and fractional cloud cover. This last parameter was probably below 100% because cloud formation may have been inhibited in regions of atmospheric subsidence. Surface temperatures calculated assuming a 75% fractional cloud cover with visible optical depth $\tau = 10$ were found to be 20 to 30 K colder than those for a 100% cloud cover. It might be expected that clear sky regions were harder to maintain on early Mars than on modern Earth, as the clouds in the former case arise from condensation of the atmosphere's primary constituent, whence subsidence must maintain anomalously warm conditions in a deep layer to inhibit condensation. The issue of fractional cloud cover is an important one that is inextricably tied up with dynamics and can only be treated in the context of a full 3D climate model.

Eventually, without taking into account the additional effect of water clouds, we found that a surface pressure lower than 1 bar may have been sufficient to raise the global mean temperature of early Mars to the melting point of water (Fig. 4). In fact, it has been suggested that the geomorphic observations on Mars can be explained with mean temperatures a few tens of degrees below freezing (*3*, *22*). According to Fig. 4, this would allow a surface pressure as low as 0.3 bar or a mean cloud optical depth of only 1. In any case, conditions suitable for life could easily have been reached. The requirement for life is the presence of liquid water, regardless of mean temperature and pressure. As seen in Earth's polar regions, major liquid water habitats supporting life can be maintained by the insulating properties of an ice cover or by geothermal activity, even when temperatures are well below freezing (*22*).

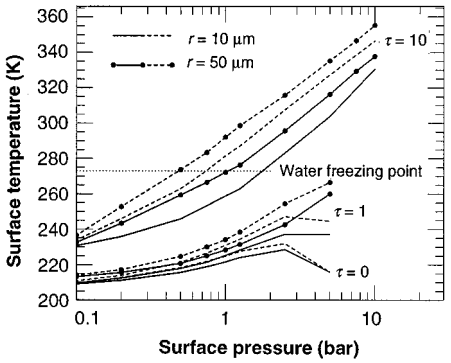

Fig. 4. Mean surface temperature as a function of surface pressure for several values of the mean cloud τ in the cases of a wet (dashed curves) or dry (solid curves) CO_2 atmosphere on Mars. A 25% reduced luminosity is assumed.

The high surface temperatures (Fig. 4) indicate that the greenhouse effect of a thick, wet, condensing CO_2 atmosphere can be extremely powerful. This general mechanism should be taken into account in the estimation of the "habitable zone" (suitable for life on extrasolar planets) around stars. For instance, a wet 10-bar CO_2 atmosphere filled with $\tau = 10$ CO_2 ice clouds would allow a mean surface temperature above the freezing point of water at more than 2.4 astronomical units (AU) from a sunlike star, beyond the outer edge of the habitable zone found by Kasting *et al.* (*23*) at 1.37 AU. Similarly, CO_2 ice clouds may have played a role in warming Earth when the sun was fainter than today (*24*), assuming that enough CO_2 was available on early Earth (*5*). As for Mars, given our current knowledge of the environmental conditions 3.8 billion years ago, our conclusions must remain speculative. Nevertheless, it must be emphasized that our CO_2 ice cloud scenario is simple. It does not require any ad hoc combination of physical processes. Assuming that the atmosphere was composed of more than a few 0.1 bar of CO_2, it is likely that CO_2 clouds formed and that they contributed to warming the planet enough for liquid water to flow on the surface.

REFERENCES AND NOTES

1. J. B. Pollack, J. F. Kasting, S. M. Richardson, K. Poliakoff, *Icarus* **71**, 203 (1987); F. P. Fanale, S. E. Postawko, J. B. Pollack, M. H. Carr, R. O. Pepin, in *Mars*, H. H. Kieffer, B. M. Jakosky, C. W. Snyder, S. M. Matthews, Eds. (Univ. of Arizona Press, Tucson, AZ, 1992), pp. 1135–1179.
2. J. F. Kasting, *Icarus* **94**, 1 (1991).
3. S. W. Squyres and J. F. Kasting, *Science* **265**, 744 (1994).
4. D. P. Whitmire, L. R. Doyle, R. T. Reynolds, J. J. Matese, *J. Geophys. Res.* **100**, 5457 (1995).
5. J. F. Kasting, *Science* **276**, 1213 (1997).
6. C. Sagan and C. Chyba, *ibid.*, p. 1217.
7. G. B. Hansen, *J. Geophys. Res.* **102**, 21569 (1997).
8. O. B. Toon, C. P. McKay, T. P. Ackerman, K. Santhanam, *ibid.* **94**, 16287 (1989).
9. Mie theory assumes spherical particles. Nonsphericity of ice particles affects scattering asymmetry. However even for Earth cirrus clouds, where much is known about crystal shape, Mie theory is commonly used because the associated errors are subsidiary to other poorly represented aspects of cloud physics (*10*). For early Mars, where hardly anything is known about the crystal growth habits, there is even less basis for going beyond Mie theory.
10. G. L. Stephens, S.-C. Tsay, P. W. Stackhouse, P. J. Flatau, *J. Atmos. Sci.* **47**, 1742 (1990); E. J. Jensen, S. Kinne, O. B. Toon, *Geophys. Res. Lett.* **21**, 2023 (1994).
11. Martian gravity is weaker than Earth's gravity, but CO_2 ice is denser than water ice, and the viscosity of CO_2 gas at the CO_2 ice cloud temperatures is lower than for the air in Earth's cirrus clouds.
12. J. A. Stansberry, R. M. Haberle, C. P. McKay, presentation at the 27th Annual Meeting of the Division for Planetary Science of the American Astronomical Society, Hawaii, 9 October 1995.
13. R. E. Samuelson, *Astrophys. J.* **147**, 782 (1967).
14. F. Forget, J. B. Pollack, G. B. Hansen, *J. Geophys. Res.* **100**, 21119 (1995).
15. J. B. Pollack *et al.*, *Icarus* **103**, 1 (1993).
16. C. P. McKay, J. B. Pollack, R. Courtin, *ibid.* **80**, 23 (1989).
17. F. Forget and J. B. Pollack, *J. Geophys. Res.* **101**, 16865 (1996).
18. The original radiative transfer model is described in detail in (*2*) and in J. F. Kasting, J. B. Pollack, T. P Ackerman, *Icarus* **57**, 335 (1984). IR absorption is calculated in 55 spectral intervals ranging from 0.54 to 500 μm, using 25 vertical layers. The original code was only designed for pure absorption. For instance, the upward component of the spectral intensity I_0 in a given band at level z was

$$I_0(z,\mu) = B(z_s)e^{-\tau(z\ldots z_s,\mu)} + \int_z^{z_s} B(z')e^{-\tau(z\ldots z',\mu)}\frac{d\tau}{dz'}\,dz' \quad (1)$$

where μ is the cosine of the zenith angle, $B(z)$ is the Planck function at level z (z_t at the top of the atmosphere; z_s at the surface), and $\tau(z\ldots z',\mu)$ is the slant opacity between levels z and z'. Clouds were introduced in the model by modifying the upward and downward IR fluxes above and below the cloud, respectively. The contribution from across the cloud was reduced by the cloud band transmissivity β and increased by the reflection and emission of the cloud of reflectivity α and emissivity ϵ. For instance, the upward intensity above the cloud level z_c became

$$I(z,\mu) = \beta I_0(z,\mu) + (1-\beta)\int_z^{z_c} B(z')e^{-\tau(z\ldots z',\mu)}\frac{d\tau}{dz'}\,dz' - \alpha\int_{z_t}^{z_c} B(z')e^{-\tau(z'\ldots z_c\ldots z_t,\mu)}\frac{d\tau}{dz'}\,dz' + \epsilon B(z_c)e^{-\tau(z\ldots z_c\mu)} \quad (2)$$

Applying this method, we neglected the enhanced gaseous absorption that can occur in multiple scattering clouds. However, because IR radiation scattering by CO_2 ice is important at wavelengths where the CO_2 gas is relatively transparent (especially at the expected cloud pressure levels on Mars), we believe that this simplification did not affect our calculations, except perhaps in the 15-μm band wings. In any case, the omission is acceptable because by neglecting this additional CO_2 gas opacity, we tend to underestimate the gas greenhouse effect and thus the surface temperature increase due to CO_2 clouds.
19. The δ-Eddington solar scattering calculation was based on (*8*), using 5619 spectral intervals covering the solar range and 100 layers in the vertical. Cloud scattering parameters were computed with the use of Mie theory with optical data from (*7*), and near-IR absorption and Rayleigh scattering representations were the same as used in (*2*). The Newton's method iteration referred to in (*2*) was found to converge unreliably in the presence of CO_2 condensation. Rather than adopting the isothermal-stratosphere approach used in (*2*), we used a time-stepping scheme similar to that in S. Manabe and R. T. Wetherald, [*J. Atmos. Sci.* **24**, 241 (1967)], in which the model is integrated as an initial value problem until it reaches equilibrium. Convergence to equilibrium was reliable but typically required several hundred time steps even when adaptively adjusted time-stepping was used to accelerate convergence. In contrast, the Newton's method iteration, when it works, converges in a dozen or fewer iterations.
20. Moisture affects both IR opacity and lapse rate. In

our "dry" calculation, we zeroed out the radiative effects of water vapor but still used the moist adiabat for the tropospheric temperature profile. This corresponds to the typical practice in radiative-convective modeling of using the moist adiabat even in highly subsaturated conditions, as in (*2*). On Earth, it is known that a moist adiabat can be maintained even if the relative humidity is low almost everywhere in the atmosphere [K. A. Emanuel, J. D. Neelin, C. S. Bretherton, *Q. J. R. Meteorol. Soc.* **120**, 1111 (1994); K. M. Xu and K. A. Emanuel, *Mon. Weather Rev.* **117**, 1471 (1989)]. Our use of the moist adiabat is a conservative choice from the standpoint of surface warming. A totally dry planet would likely adjust to the dry adiabat, which is steeper and would yield slightly greater surface temperatures than the "dry" case we show.

21. Adding 10% in mass of 10-μm water ice particles to the cloud of Fig. 2 [particle radius (r) = 10 μm; τ = 10] reduces the absorbed solar energy by 2 W m^{-2} and the scattering radiative forcing by 1.5 W m^{-2} but increases the absorption-emission forcing by 8.5 W m^{-2}, resulting in a 1.5 K surface warming. However, the effect of the water ice particles depends on their temperature. A lower, thicker water cloud would slightly cool the surface.
22. C. P. McKay, *Origins Life Evol. Biosphere* **27**, 263 (1997).
23. J. F. Kasting, D. P. Whitmire, R. T. Reynolds, *Icarus* **101**, 108 (1993).
24. K. Cadeira and J. F Kasting, *Nature* **359**, 226 (1992).
25. We thank J. Kasting for lending us his model and for helpful comments and suggestions; and J.-L. Dufresne, R. Fournier, C. McKay, and B. Weare for their advice. R.T.P. gratefully acknowledges the support of the John Simon Guggenheim Foundation and of NSF (grant ATM-9505190).

11 August 1997; accepted 6 October 1997

Mechanism for the Green Glow of the Upper Ionosphere

Steven L. Guberman

The generation of the green line of atomic oxygen by dissociative recombination of O_2^+ occurs by the capture of an electron into a repulsive state of O_2 followed by dissociation along another state of a different electronic symmetry. The two states are coupled together by mixed symmetry Rydberg states. Quantum chemical calculations give a rate coefficient at room temperature of $(0.39^{+0.31}_{-0.19}) \times 10^{-8}$ cubic centimeters per second. The quantum yield of excited oxygen is within the range deduced from ground, rocket, and satellite observations. The rate coefficients and yields are needed in models of the optical emission, chemistry, and energy balance of planetary ionospheres.

The dissociative recombination (DR) of O_2^+ with an electron (e^-), $O_2^+ + e^- \rightarrow O + O$, is an important process in the ionospheres of Mars (*1*), Venus (*2*), and Earth (*3*). At Mars, DR can provide sufficient energy to the product O atoms to allow them to escape the atmosphere (*1*). In combination with the escape of hydrogen atoms, DR has been proposed as one of several nonthermal mechanisms for the disappearance of water from the Martian surface (*1*). At Venus, the collision of H atoms with energetic O atoms produced by DR can result in the escape of H from the atmosphere (*4*). At all three planets, one of the product O atoms can be generated in the excited ^1S state, which is the source of the green airglow (caused by the ^1S to ^1D transition at 5577 Å) near 300 km in the terrestrial atmosphere (*3, 5–7*). At Earth, numerous ground, rocket, and satellite studies have reported an ionospheric O(^1S) quantum yield [that is, the number of O(^1S) atoms produced for every two product atoms] from DR of between 0.01 and 0.23 (*3, 5–7*). On the other hand, theoretical calculations with the assumed mechanisms for DR have given O(^1S) quantum yields from the lowest ion vibrational level of 0.0016 (*8*) and 0.0012 (*9*). These results have led to the suggestion that another process is generating O(^1S) in the ionosphere, although none could be identified (*10*). The DR mechanism for the generation of O(^1S) in the ionosphere and in planetary atmospheres has remained unknown.

I have shown that there is only one dissociative O_2 potential curve, $^1\Sigma_u^+$, that produces O(^1S) from the low vibrational levels of O_2^+ (*11*). The $^1\Sigma_u^+$ and ion potential curves (Fig. 1) cross between the $v = 1$ and $v = 2$ vibrational levels (v is the vibrational quantum number). The first calculation (*8*) of the rate coefficient included only the direct (*12*) recombination mechanism (Fig. 1), in which the electron is captured into the repulsive state without populating any intermediate states. Once captured, the electron can be emitted (autoionization), or the molecule can dissociate along the repulsive potential. The direct cross section and rate constant are approximately proportional to the square of the overlap between the continuum vibrational function for the $^1\Sigma_u^+$ repulsive channel and the bound ion vibrational wave function. For $v = 0$, direct capture into $^1\Sigma_u^+$ at low electron energies (for example, ε in Fig. 1) occurs in the nonclassical region, where this overlap is small. The calculated quantum yield for O(^1S) was 0.0016. Later calculations (*9*) included the indirect (*13*) recombination mechanism (Fig. 1). In indirect recombination, $O_2^+ + e^- \rightarrow O_2(RYD) \rightarrow O + O$, intermediate neutral Rydberg (RYD) states are populated that are predissociated by the same dissociative state used in the direct mechanism. These calculations gave a quantum yield for O(^1S) of 0.0012, which is smaller than the earlier results because of destructive interference between direct and indirect recombination and an order of magnitude below the yields derived from atmospheric observations.

An assumption common to all previous calculations of the DR mechanism is that molecular dissociation occurs along the same repulsive potential involved in the initial electron capture in direct DR (Fig. 1). The interaction between states of different electronic symmetries has never been accounted for in the DR mechanism. Only five states in addition to $^1\Sigma_u^+(^1S + {}^1D)$ can provide routes for DR from the low vibrational levels of the ion, $^3\Pi_u(^3P + {}^3P)$, $^1\Pi_u(^3P + {}^3P)$, $^3\Sigma_u^-(^3P + {}^1D)$, $^1\Delta_u(^1D + {}^1D)$, and $^1\Sigma_u^-(^3P + {}^3P)$ (where the states of the product atoms are shown in parentheses) (*11*). All of these curves, except $^1\Sigma_u^-$ and $^1\Pi_u$, cross the ion potential curve between the turning points of the $v = 0$ vibrational level and have more favorable initial capture probabilities than that of $^1\Sigma_u^+$, the only channel that yields O(^1S).

A small interaction usually neglected in these calculations is spin-orbit coupling, the interaction of the magnetic field

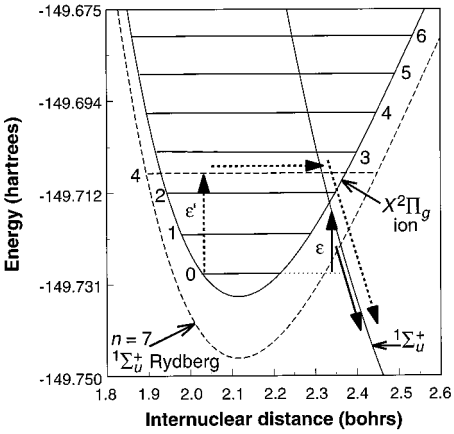

Fig. 1. Mechanisms of DR for dissociation along the $^1\Sigma_u^+$ route. Direct recombination is shown by the solid arrows at electron energy ε. Indirect recombination is shown by the dashed arrows at electron energy ε′. Also shown are the $v = 4$ vibrational level of the $n = 7$ $^1\Sigma_u^+$ potential curve (dashed lines) and the lowest seven vibrational levels of the ion (solid lines).

Institute for Scientific Research, 33 Bedford Street, Lexington, MA 02173, USA. E-mail: slg@sci.org